Nonlinear Oscillations for Cyclic Movements in Variable Impedance Actuated Robotic Arms

Dominic Lakatos, Florian Petit, and Alin Albu-Schäffer

***Abstract*—Biologically inspired Variable Impedance Actuators (VIA) offer the capability to execute cyclic and/or explosive multi degree of freedom (DoF) motions efficiently by storing elastic energy. This paper studies the preconditions which allow to induce robust cyclic motions for strongly nonlinear, underactuated multi DoF robotic arms. By experimental observations of human motor control, a simple control law is deduced. This controller achieves intrinsic oscillatory motions by switching the motor position triggered by a joint torque threshold. Using the derived controller, the periodic behavior of the robotic arm is analyzed in simulations. It is found that a modal analysis of the linearized system at the equilibrium point allows to qualitatively predict the periodic behavior of this type of strongly nonlinear systems. The central statement of this paper is that cyclic motions can be induced easily in VIA systems, if the eigenfrequencies and modal damping values of the linearized system are well separated. Validation is given by simulation and experiments, where a human controls a simulated robotic arm, and the developed regulator controls a robotic arm in simulation and experiments.**

I. Introduction

Humans execute easily high-performance cyclic movements such as running or drumming or explosive motions such as throwing, hitting or jumping. To approach human athletic performance and efficiency, robot design evolved recently from classical, rigid actuation towards actuators with tunable intrinsic stiffness and/or damping, so called Variable Impedance Actuators (VIA). These elastically actuated robots are strongly inspired by the biological musculo-skeletal system [1]. They are motivated by biomechanics research which reveals the importance of the elasticity for robustness and energetic efficiency as well as for the maximization of peak force and velocity [2]. The goal is to exploit intrinsic mechanical resonance effects of the systems.

The generation of motor trajectories and the tuning of joint stiffness during these highly dynamic motions are often addressed as an optimal control problem. While for single joints an analytical solution is feasible [3] , [4], for the multi-joint case numerical, multi-variable constrained optimizations need to be performed [5], [6]. The optimization approach is currently limited to systems with few degrees of freedom (DoF). With an increasing number of degrees of freedom (for example in the case of one arm (7 DoF) or even a humanoid body (> 30 DoF)) the computational complexity and the number of local minima explodes. This motivates the investigation of alternative approaches.

The authors are with the Robotics and Mechatronics Center (RMC) – Institute of Robotics and Mechatronics, German Aerospace Center (DLR), D-82234 Oberpfaffenhofen, Germany {dominic.lakatos, florian.petit, alin.albu-schaeffer}@dlr.de.

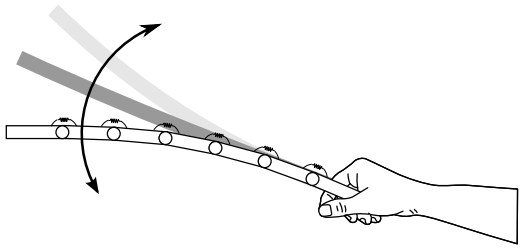

Fig. 1. Human induces cyclic movements for a rod with nonlinear elasticities

In this paper we focus on the generation of cyclic motions. It is a known fact that un-damped, elastic multi-body systems tend to show chaotic behavior. In particular, the response of such systems to sinusoidal excitation is not necessarily periodic [7], [8]. This motivates us asking under which conditions a VIA robot (and a human) arm can display periodic motions, how easily they can be induced and how robustly they can be stabilized. *Simple experiments with passive systems (Fig. 1) suggest that humans can easily induce such nonlinear oscillations.* Despite the current theoretical difficulties, for instance, the complexity of an associated optimal control problem to reach periodic motions, humans seem to be able to excite independent nonlinear oscillatory modes of the system without difficulty.

The above hypothesis is verified by means of hardware in the loop simulations, where a human controls a real-time simulation of a VIA arm using a force feedback device. The inertia of the arm and the visco-elastic parameters of the joints are varied within consecutive trials to evaluate their influence on the limit cycles. An important finding of the experiments is that the existence of easily excitable cyclic motions is predominantly determined by the system's damping properties. Although the original system is strongly nonlinear, damping analysis of the eigenmodes, based on linearization at the equilibrium point, already allows to predict whether the intrinsic system behavior tends to first mode cyclic motions or not. If the modal damping factors of the linearized system are sufficiently different, a simple multi-step bang-bang feedback controller achieves coordinated cyclic motions.

In addition to simulation experiments, we verify the approach on a real VIA system. This way, we close the loop from hypotheses to verification using simulations, human in-the-loop experiments, and robotic experiments.

This paper is organized as follows: First, the considered robotic system is introduced and the model nonlinearities are emphasized. Then, the problem is stated and main hypotheses are proposed in Section III. To validate our hypotheses with

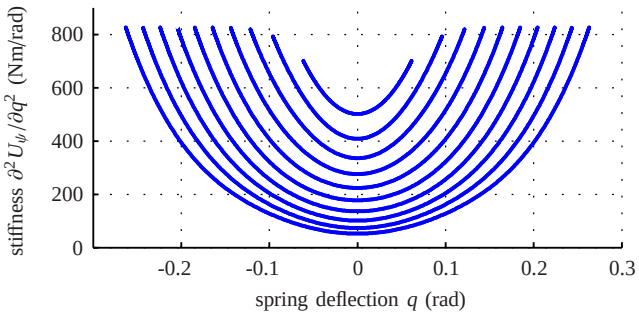

Fig. 2. Stiffness of the floating spring mechanism (as used in the DLR Hand Arm System) for constant adjuster positions $\theta_\psi = \{0, 0.02, 0.04, 0.06, 0.08, 0.10, 0.12, 0.14, 0.16, 0.18\}$. The most outer curve corresponds to $\theta_\psi = 0$.

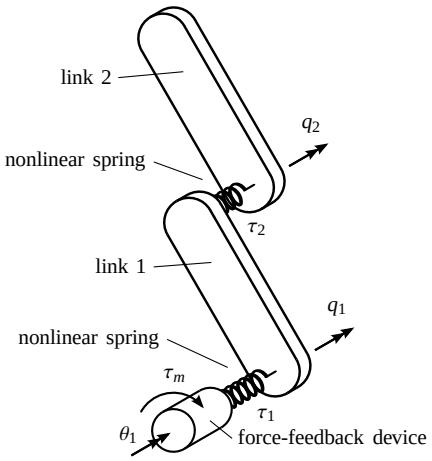

Fig. 3. Technical scheme of the hardware in the loop simulation. The complete system: double pendulum including nonlinear visco elasticities is simulated in real time. Position θ_1 and/or velocity $\dot{\theta}_1$ of the feedback device is a control input. The joint torque τ_1 of the first joint acts as force feedback.

experiments, two main steps are performed. In Section III qualitative system requirements for multi degree of freedom oscillations are deduced from experiments, where a *human* controls a *robotic arm*. Furthermore a simple bang-bang controller is proposed based on the analysis of the human behavior. In Section IV and V the case where the bang-bang *controller* induces oscillations in a *robotic arm* is considered and the influence of modal parameters on nonlinear oscillations is analyzed by both, simulation and experiment. Finally, properties of the bang-bang controller are discussed and a brief conclusion is given in Section VI.

II. Nonlinearities in variable impedance actuated robots

The main goal of this paper is to understand cyclic motions of VIA systems for controlling robots. This class of nonlinear, underactuated systems can be generally described by dynamic equations of the form [9], [10]:

$$\boldsymbol{M}(\boldsymbol{x})\ddot{\boldsymbol{x}} + \boldsymbol{c}(\boldsymbol{x}, \dot{\boldsymbol{x}}) + \frac{\partial U(\boldsymbol{x})}{\partial \boldsymbol{x}} = \boldsymbol{Q} \,. \tag{1}$$

Herein $\boldsymbol{x}, \dot{\boldsymbol{x}}, \ddot{\boldsymbol{x}} \in \mathbb{R}^n$ are generalized coordinates and their time derivatives, respectively. $\boldsymbol{Q} \in \mathbb{R}^n$ is a non-conservative, generalized force dual to $\dot{\boldsymbol{x}}$. The potential energy

$$U(x) = U_g(\boldsymbol{x}) + U_\psi(\boldsymbol{x}) \,, \tag{2}$$

is in general composed of the gravity potential $U_g(\boldsymbol{x})$ and the spring potential $U_\psi(\boldsymbol{x})$. Furthermore $\boldsymbol{M}(\boldsymbol{x}) \in \mathbb{R}^{n\times n}$ is the symmetric and positive definite mass matrix and $\boldsymbol{c}(\boldsymbol{x}, \dot{\boldsymbol{x}}) \in \mathbb{R}^n$ a vector of Coriolis/centrifugal forces.

The design of VIA robots involves that not all of the system states are directly actuated. Therefore, let us partition the states $\boldsymbol{x} = (\boldsymbol{\theta}, \boldsymbol{q})$ as $\boldsymbol{\theta} \in \mathbb{R}^k$ being directly actuated states (referred to as motor positions) and $\boldsymbol{q} \in \mathbb{R}^{n-k}$ being indirectly actuated states (referred to as link positions). Additionally, let us consider linear viscous damping $\boldsymbol{D}\dot{\boldsymbol{x}}$ (where $\boldsymbol{D} \in \mathbb{R}^{n\times n}$ is the symmetric and positive definite damping matrix), then the generalized force

$$\boldsymbol{Q} = \begin{bmatrix} \boldsymbol{\tau}_m \\ \boldsymbol{\tau}_{ext} \end{bmatrix} - \boldsymbol{D}\dot{\boldsymbol{x}} \tag{3}$$

consists of the control input $\boldsymbol{\tau}_m \in \mathbb{R}^k$ and the externally applied force $\boldsymbol{\tau}_{ext}$. Since the dimension of the control input is smaller than the state dimensionality, the systems is underactuated. The gradient of the potential energy can be separated into:

$$\frac{\partial U(\boldsymbol{x})}{\partial \boldsymbol{x}} = \begin{bmatrix} \dfrac{\partial U(\boldsymbol{\theta}, \boldsymbol{q})}{\partial \boldsymbol{\theta}} \\ \dfrac{\partial U(\boldsymbol{\theta}, \boldsymbol{q})}{\partial \boldsymbol{q}} \end{bmatrix} . \tag{4}$$

As can be seen from (1) and (4) the states $\boldsymbol{\theta}$ and $\boldsymbol{q}$ are coupled via the elastic energy storage $U_\psi(\boldsymbol{\theta}, \boldsymbol{q})$. This energy storage is an important precondition to induce cyclic motions on $\boldsymbol{q}$ efficiently.

Variable stiffness actuation usually entails strong nonlinearities to the system dynamics. For example, for the DLR Hand Arm System [11], variable stiffness actuation is realized by so-called floating spring joints [12]. Therein, the spring potential of a single joint can be approximated by a fourth order polynomial

$$U_\psi(\boldsymbol{\theta}, q) = \frac{1}{2}\alpha(\theta_\psi)\left(q - \theta_q\right)^2 + \frac{1}{4}\beta(\theta_\psi)\left(q - \theta_q\right)^4 \tag{5}$$

and the force-deflection relation is then given by

$$\psi(\boldsymbol{\theta}, q) \coloneqq \frac{\partial U_\psi(\boldsymbol{\theta}, q)}{\partial q} = \alpha(\theta_\psi)\left(q - \theta_q\right) + \beta(\theta_\psi)\left(q - \theta_q\right)^3 , \tag{6}$$

where $\boldsymbol{\theta} = (\theta_q, \theta_\psi)$ are the motor positions of the main actuator and the stiffness adjuster, respectively. To display the order of nonlinearity introduced due to the variable stiffness actuation, the stiffness $\partial^2 U_\psi(\boldsymbol{\theta}, q)/\partial q^2(\theta_q = 0)$ of the mechanically implemented floating spring joint is plotted in Fig. 2 for several stiffness presets. In the case of the lowest preset $\theta_\psi = 0$ the variation is about 1480% between minimum and maximum spring deflections. Note that the joint stiffness is changing with the joint deflection. Additionally, the stiffness preset can be changed by the stiffness adjuster motors.

III. Controller design inspired by human motor control

Simple experiments were conducted, where a human induces oscillations into a rod (see, Fig. 1). Stable oscillations

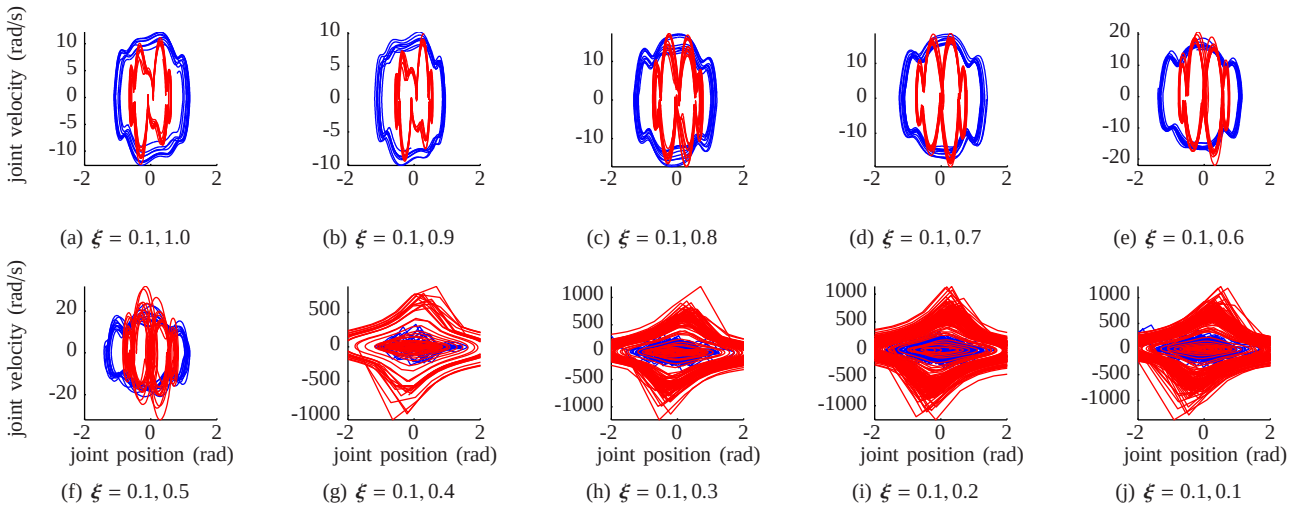

Fig. 4. Phase plots of human controlled oscillations. Blue lines represent the pair $(q_1, \dot{q}_1)$ and red lines the pair $(q_2, \dot{q}_2)$. The eigenfrequecies $\omega_1(\mathbf{0}) = 1.9\,(\text{rad/s})$ and $\omega_2(\mathbf{0}) = 20.9\,(\text{rad/s})$ were constant over all trials, while the modal damping factors $\boldsymbol{\xi}(\mathbf{0})$ had been varied.

could be achieved even for the case of large deflections (i.e. in the emergence of strong nonlinearities). The human does not need a long training phase to do so. This demonstrates human's ability to control periodic motions of nonlinear multi degree of freedom systems. From these observations we hypothesize that:

- Human's motor control is able to stabilize periodic motions even in the presence of strong nonlinearities.
- The underlying control law has a simple and very robust structure.

To verify both hypotheses, several experiments involving VIA arms, human dynamics, and human control have been conducted.

Accessing and measuring human's control and feedback signals during natural motions is difficult and largely unresolved [13]. We circumvent this problem by using hard- and software in the loop simulations with human control. Using a force feedback device, a human operator can be coupled in the feedback control loop with either a robotic plant or a simulated system. The latter allows to adjust the system parameters arbitrarily as done in the following experiments.

A. Model simplification

To include the force feedback device in the control loop using one of the robot's motor position and/or velocity as control input, the general dynamic model (1) is customized based on simplifying assumptions widely applied in robotics. These simplifying assumptions are fully justified for the DLR Hand Arm System and briefly summarized as following:

- the coupling inertias in between motor and link side can be neglected[1].
- The motor side dynamics is faster than the link side dynamics such that the motor position can be considered as control input[2].

[1]This assumption is fulfilled in the presence of high gear ratios, cf. [14].
[2]This assumption is used in singular perturbation theory, cf. e.g. [15], [16].

Furthermore, in the following experiments, the stiffness preset of the VIA joints will be changed only statically. Accordingly, the simplified dynamic equations have the form:

$$\boldsymbol{M}_q(\boldsymbol{q})\ddot{\boldsymbol{q}} + \boldsymbol{c}_q(\boldsymbol{q}, \dot{\boldsymbol{q}}) + \frac{\partial U_g(\boldsymbol{q})}{\partial \boldsymbol{q}} = -\frac{\partial U_\psi(\boldsymbol{\theta}, \boldsymbol{q})}{\partial \boldsymbol{q}} + \boldsymbol{Q}_q \,. \quad (7)$$

For further analysis, the motion in a plane perpendicular to the gravity is considered, i.e. $\partial U_g(\boldsymbol{q})/\partial \boldsymbol{q} \equiv \mathbf{0}$. Damping acts only on the link side:

$$\boldsymbol{Q}_q = -\boldsymbol{D}_q \dot{\boldsymbol{q}} \,. \quad (8)$$

As control input we use $u := \theta_1$, while $\theta_2, \ldots, \theta_k = 0$ are kept constant and the feedback control developed later on is based on the first joint torque $\tau_1 := -\partial U_\psi(\boldsymbol{\theta}, \boldsymbol{q})/\partial q_1$.

For convenience of notation, subscripts $(\cdot)_q$, used to denote link side terms (see, e.g. (7)), are omitted in the remainder of the paper.

B. Experiments

The real time simulation of (7) was interconnected with a direct drive (torque controlled) motor with a handle mounted on the rotor. This motor acts as force feedback device. An optical encoder provides the angular position of the motor as control signal $u := \theta_1$ for the simulated VIA arm. The joint torque τ_1 computed by the VIA arm simulation is commanded to the current controller of the force feedback device and thereby provides feedback to the human operator. This setup allows to emulate arbitrary dynamical systems that are controlled by a single position input, and interface them to a human operator.

In a series of experiments, the oscillatory behavior of a VIA double pendulum (i.e., $\boldsymbol{q} \in \mathbb{R}^2$, $\boldsymbol{\theta} \in \mathbb{R}^2$, $u := \theta_1$, and $\theta_2 = 0$) was analyzed (see, Fig. 3). Besides inertial dynamics, strong nonlinear cubic springs (cf. (6)) were considered, where the ratio of linear and cubic spring constants was chosen as $\beta_i/\alpha_i = 70$ (similar to the most nonlinear case of the floating spring mechanism, cf. Fig. 2). To comply with the

range of maximum torques of the force feedback device $\tau_{max} = \pm 1\,\mathrm{Nm}$, inertia and spring parameters were adjusted: mass $m_{1/2} = 0.1\,\mathrm{kg}$, link length $l_{1/2} = 0.1\,\mathrm{m}$, center of mass $l_{ci} = l_i/2$, $\alpha_1 = 0.02\,\mathrm{Nm}$, and $\alpha_2 = 0.01\,\mathrm{Nm}$. The knowledge of the stiffness and mass matrix of the linearized system allows to assign a modal damping coefficient $0 \le \xi \le 1$ (see (20) in the Appendix). The system (7) was integrated (forward Euler method, time steps 0.001 s) on the same real time computer on which the force feedback device was controlled. Additionally, the motion of the double pendulum was visualized on a screen.

One skilled participant was tested at random with different system parameters. During all tests, the subject grasped the handle of the force feedback device and rested in the initial position, while the integrator was reseted. Then the subject moved the handle to induce oscillations. The goal was to achieve and stabilize coordinated, cyclic movements.

C. Results

Given the physically motivated setup, it was straightforward for the subject to stabilize cyclic movements. Even more, the system tends to show only first mode motions. The modal analysis of the linearized system revealed that the first eigenmode is less damped than the second one. This finding was further validated by directed tests, where the normalized damping factor of the first mode was held low and constant, while the damping factor of the second mode has been varied. Phase plots of the joint motion $\boldsymbol{q}(t)$ vs. $\dot{\boldsymbol{q}}(t)$ are displayed in Fig. 4.

1) The influence of modal damping: Nonlinear effects—induced by inertia couplings, Coriolis effects and the progressive stiffness characteristic of the springs—increase when the damping of the second mode converges to the first mode damping factor. These effects are expressed in form of strong notches towards the center in the shape of circular or elliptical paths. Severe changes occur when the damping of the second mode falls below approximately 0.5; then numerical instabilities of the simulation arise (cf. 4(g)–(j)).

2) The steady-state of cyclic motions: For ideal cyclic motions a phase plot trajectory of one state is a single closed path, while the trajectories depicted in Fig. 4 lie within an error band. The reason therefore can be limitations in the range and sensitivity of feedback signals given to the human operator. Additionally, the control signals generated by humans may not be sufficiently accurate and repeatable. The deterministic controller proposed next allows to avoid these uncertainties.

D. A multi-step bang-bang controller

From qualitative observations of the human control strategy a simple control law has been deduced. It was observed that when the spring deflection reached a torque peak, the human countered it by pushing harder in the opposite direction of the link side motion and thereby induced energy into the system. Such a behavior can be approximately replicated by the discontinuous control law:

$$\theta_d = \begin{cases} \theta_0 + \mathrm{sign}(\tau)|\hat{\theta}| & : |\tau| > \epsilon_\tau \\ \theta_0 & : \text{else} \end{cases} . \qquad (9)$$

As depicted in Fig. 5, this multi step bang-bang controller is triggered by the feedback torque τ. When τ exceeds a certain threshold ϵ_τ the controller gives an impulse in the same direction of the observed torque. This is achieved by a step $\hat{\theta}$ in motor position w.r.t. the initial position θ_0.

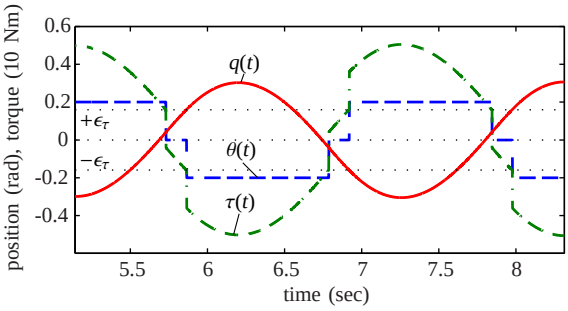

Fig. 5. Action principle of the multi-step bang-bang controller depicted as time plot.

IV. Dynamic system properties for cyclic motion: Simulations

In the last section it was demonstrated that even in the presence of strong nonlinearities, multi degree of freedom cyclic movements can be induced easily by a human. Now, we investigate intrinsic system properties, which ensure that the system tends to periodic motions.

In more detail, the system considered is the VIA pendulum of the form (7) with cubic springs defined by (6) in the joints, where the first joint's motor position $u := \theta_1$ acts as control input and the elastic torque $\tau_1 := -\partial U_\psi(\boldsymbol{\theta}, \boldsymbol{q})/\partial q_1$ is used as feedback. (The remaining motor position $\theta_2 = 0$ is hold constant.) To obtain repeatable results, oscillations are induced by means of the control law (9) instead of the human operator. The controller parameters are set to $\hat{\theta} = 0.3\,\mathrm{rad}$ and $\epsilon_\tau = 30\,\mathrm{Nm}$ for all simulations. Although the considered system is nonlinear, the spring and damping parameters will be adjusted based on linearization at the equilibrium point. For the link side mass matrix at zero position $\boldsymbol{M}(\boldsymbol{0})$ fixed, desired eigenfrequencies are assigned (given below for specific cases), in order to compute the linear spring coefficients α_i. Then the physical damping is computed based on the linearized stiffness matrix and given modal damping factors (see, Appendix). Finally, coefficients of cubic spring terms are chosen such that $\beta_1/\alpha_1 = \beta_2/\alpha_2 = 70$.

All simulations were performed in Matlab/Simulink®. The differential equations were integrated by means of the variable step solver ode23t for moderately stiff problems with a maximum step size of 0.0005 sec. Initial conditions were set $(0.6, 0)$ for joint angles and $(0, 0)$ for joint velocities.

A. Limit cases of modal properties

Based on the inertial properties of the DLR Hand Arm System, two substantially different cases of eigenfrequency distributions are considered:

1) Different eigenfrequencies: As in the case of the DLR Hand Arm System most of the VIA robots are mono-articulated, i.e. no coupling springs are present. In more detail, a displacement in the single direction of one joint generates solely a reaction force in the opposite direction of the same

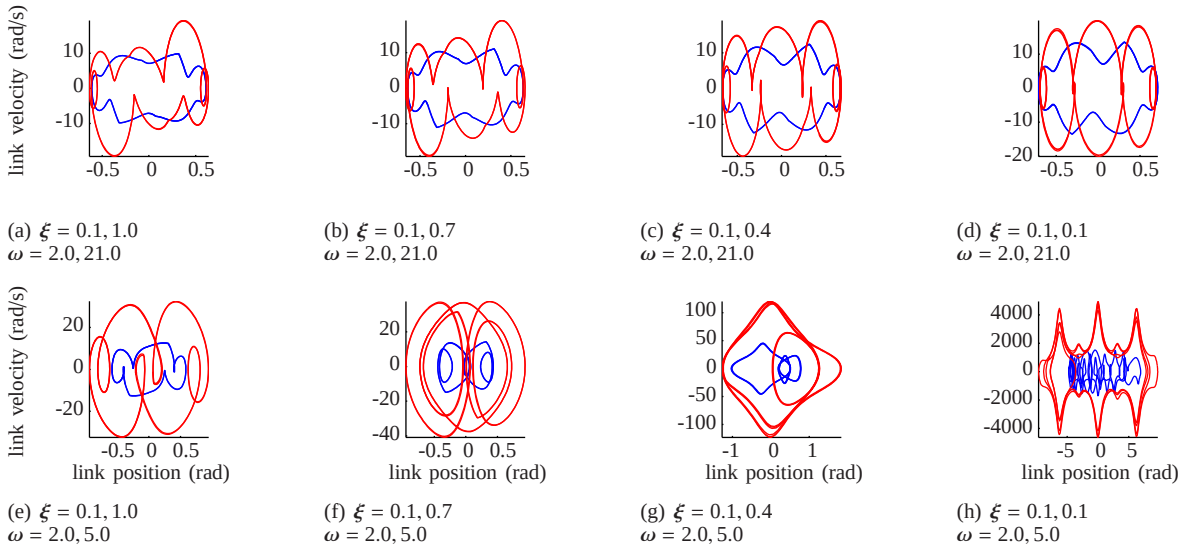

(a) $\boldsymbol{\xi} = 0.1, 1.0$ $\boldsymbol{\omega} = 2.0, 21.0$ (b) $\boldsymbol{\xi} = 0.1, 0.7$ $\boldsymbol{\omega} = 2.0, 21.0$ (c) $\boldsymbol{\xi} = 0.1, 0.4$ $\boldsymbol{\omega} = 2.0, 21.0$ (d) $\boldsymbol{\xi} = 0.1, 0.1$ $\boldsymbol{\omega} = 2.0, 21.0$

(e) $\boldsymbol{\xi} = 0.1, 1.0$ $\boldsymbol{\omega} = 2.0, 5.0$ (f) $\boldsymbol{\xi} = 0.1, 0.7$ $\boldsymbol{\omega} = 2.0, 5.0$ (g) $\boldsymbol{\xi} = 0.1, 0.4$ $\boldsymbol{\omega} = 2.0, 5.0$ (h) $\boldsymbol{\xi} = 0.1, 0.1$ $\boldsymbol{\omega} = 2.0, 5.0$

Fig. 6. Phase plots of simulated motions, where the controller proposed in Section III is in the loop. Blue lines represent the pair $(q_1, \dot{q}_1)$ and red lines the pair $(q_2, \dot{q}_2)$. Simulations displayed correspond to the mass distribution of the DLR Hand Arm System.

joint:

$$-\frac{\partial U_\psi(\boldsymbol{\theta}, \boldsymbol{q})}{\partial q_i} = \psi_i(\boldsymbol{\theta}, q_i) \; . \tag{10}$$

Linearizing these elastic force functions leads to a diagonal stiffness matrix:

$$\boldsymbol{K}(\theta, \boldsymbol{q}) = \mathrm{diag}\left(\frac{\partial^2 U_\psi(\boldsymbol{\theta}, \boldsymbol{q})}{\partial q_i^2}\right) \; . \tag{11}$$

Then, as a consequence of the coupled mass matrix (and for $\boldsymbol{q} \in \mathbb{R}^2$) there exists a minimum ratio of assignable eigenfrequencies $\omega_2/\omega_1 > \nu_{\min}(\boldsymbol{M})$, which can be realized by a diagonal stiffness matrix (see, (32) in the Appendix), i.e. for a given mass matrix $\boldsymbol{M}$ and first eigenfrequency ω_1 the second eigenfrequency ω_2 must be larger than $\omega_1 \nu_{\min}(\boldsymbol{M})$, otherwise a coupled stiffness matrix is required. This (utile)-case (appropriate for VIA robots without coupling springs) was considered for human controlled oscillations described in the last section.

2) Similar eigenfrequencies: In contrast to sufficiently different eigenfrequencies, the case of similar eigenfrequencies requires to introduce coupling springs. They have the effect, that a displacement in one coordinate direction can cause a reaction force in a different coordinate direction:

$$-\frac{\partial U_\psi(\boldsymbol{\theta}, \boldsymbol{q})}{\partial q_i} = \psi_i(\boldsymbol{\theta}, \boldsymbol{q}) \tag{12}$$

and consequently the stiffness matrix for the instantaneous linearized system contains nonzero, off-diagonal entries:

$$K_{i,j}(\boldsymbol{\theta}, \boldsymbol{q}) = \frac{\partial^2 U_\psi(\boldsymbol{\theta}, \boldsymbol{q})}{\partial q_i \partial q_j} \neq 0 \; . \tag{13}$$

Note that nonlinear coupling elasticities are not present in most of today's VIA robot arms, therefore we introduce this artificial case of similar eigenfrequencies here for sake of theoretical insight.

B. Simulation results

Figures 6(a)–(d) display phase plots of simulated motions for the case of different eigenfrequencies. For each simulation run eigenfrequencies $\omega_1(\mathbf{0}) = 2\,\mathrm{rad/s}$ and $\omega_2(\mathbf{0}) = 21\,\mathrm{rad/s}$ corresponding to $\nu_{\min}(\boldsymbol{M})$ in this case were assigned, while the modal damping is varied in each run. Note that ω_1 was chosen arbitrarily and ω_2 results due to $\nu_{\min}(\boldsymbol{M})$. For all presets of modal damping, phase plots of both coordinate directions are closed paths—indicating the system's tendency to cyclic movements. As in the case of human controlled oscillations the effects of nonlinearities (manifested by strong notches towards the center in the phase plots paths) increase, when the value of the second mode damping (in the equilibrium position) approaches the value of the first mode damping (in the equilibrium position). But in contrast to human controlled oscillations (see, Fig. 4(j)) the bang-bang regulator (9) avoids irregular, numerically unstable behavior. Even for the case of equal and low modal damping, the motion stays within a small error band (cf. Fig. 6(d)).

To demonstrate the strong occurrence of nonlinearities, time series of the control input $\theta_1(t)$, joint angles $\boldsymbol{q}(t)$, joint velocities $\dot{\boldsymbol{q}}(t)$, as well as instantaneous values of the modal damping $\boldsymbol{\xi}(t)$, eigenfrequencies $\boldsymbol{\omega}(t)$, and potential / kinetic energy $U(t)$ / $T(t)$ corresponding to the phase plot Fig. 6(a) are depicted in Fig. 7. It can be observed that only in the equilibrium point $\boldsymbol{q} = \mathbf{0}, \theta = 0$ eigenfrequencies and modal damping equal the assigned values. At these points the modal damping has its maximum and the eigenfrequency its minimum. For increasing magnitudes of spring deflections $|q_i - \theta_i|$ both instantaneous eigenfrequencies increase and the modal damping factors decrease. When spring deflections are maximal, the eigenfrequencies / modal damping factors approach their maxima / minima. Additionally, one can identify points where the Hamiltonian energy is almost completely kinetic. This is a typical property for coordinated cyclic movements

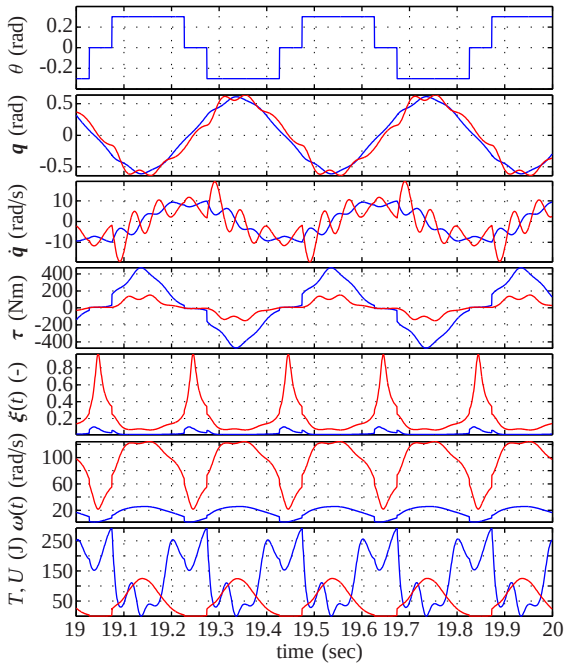

Fig. 7. Time series corresponding to the simulation plotted in Fig. 6(a). Herein θ is the motor position of the first joint, i.e. the control action. $\boldsymbol{q}$, $\dot{\boldsymbol{q}}$, and $\boldsymbol{\tau}$ are link positions, link velocities, and joint torques of the first (blue) and second (red) joint, respectively. $\boldsymbol{\xi}(t)$ and $\boldsymbol{\omega}(t)$ are instantaneous values of modal damping and eigenfrequency. System's kinetic energy T (blue) and potential energy U (red) is depicted in the last plot.

[17].

Let us now consider the case of similar eigenfrequencies. To this end, again, desired eigenfrequencies are assigned to the linearized system at the equilibrium point. Therefore, we consider the mass matrix $\boldsymbol{M}(\mathbf{0})$ as given and tune the entries of the stiffness matrix

$$\boldsymbol{K}_0 = \begin{bmatrix} \alpha_1 + \alpha_3 & -\alpha_3 \\ -\alpha_3 & \alpha_2 + \alpha_3 \end{bmatrix}. \tag{14}$$

The resulting entries of the above stiffness matrix correspond to the linear coefficients α_i of the springs. In more detail, first, the condition $\omega_2/\omega_1 < \nu_{\min}(\boldsymbol{M})$ is tested. Then it is decided if the eigenfrequencies can be achieved by a diagonal or coupled stiffness matrix[3]. For each case exists an analytical relation to determine α_i. The resulting potential function (23) as well as the force and stiffness functions are given in the Appendix. Although we adjust the linear spring coefficients α_i based on linearization (at the equilibrium point), we consider the nonlinear joint elasticities in simulation.

In simulations the procedure given in the Appendix is applied to assign the eigenfrequencies $\omega_1 = 2\,\mathrm{rad/s}$, $\omega_2 = 5\,\mathrm{rad/s}$. Therefore, the value of the cubic spring coefficient is chosen $\beta_3/\alpha_3 = 70/4$. Phase plots of simulated motions for the same damping adjustments as used above (while eigenfrequencies are fixed) are depicted in Fig. 6(e)–(h). It can be observed that even for the case in Fig. 6(e) where the first mode damping $\xi_1(\mathbf{0}) = 0.1$ and the second mode damping

[3]Note that for a coupled mass matrix the stiffness matrix has to be also coupled and even $\boldsymbol{K} \propto \boldsymbol{M}$ to have n repeated eigenvalues [17]

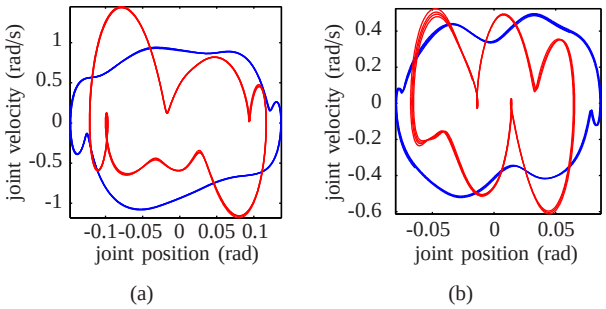

Fig. 8. Phase plots obtained from experiments on the DLR Hand Arm System. Joint positions are sampled at 3 kHz and low-pass filtered (cut-off frequency 10 Hz) before deriving the joint velocities, numerically.

$\xi_2(\mathbf{0}) = 1.0$, the first mode is not excited, isolatedly. These coupling effects are expressed in form of loop-like notches in the circular or elliptic shapes of curves. For decreasing values of the second mode damping $\xi_2(\mathbf{0})$ (decreasing between simulation runs), abrupt energy exchanges between the modes induce non-periodic behavior.

Remark 1 (Steady-state oscillations): Compared to oscillations induced by a human operator, the bang-bang regulator achieves ideal cyclic motions. While phase plots depicted in Fig. 4 deviate from ideal closed paths within a certain "error band", stable steady state motions in Fig. 6 display single, exactly closed curves for each joint coordinate. It remains open to further research, if the humans behavior is due to control imprecisions or has some other benefits.

C. Summary

Under specific conditions considered in this work, simulation results demonstrate that determining the modal parameters, i.e. eigenfrequency and damping, for the linearization of the system at the equilibrium position allows to predict the periodic behavior of this type of strongly nonlinear systems. Best preconditions for cyclic movements are different eigenfrequencies and different modal damping. This case applies to the robotic VIA arm in the absence of coupling springs. Therefore a simple controller is able to stabilize cyclic movement. Furthermore, the intrinsic system behavior is tending to first mode motions, even for similar eigenfrequencies, as long as the first eigenmode is weakly damped and the second eigenmode is strongly damped.

V. Cyclic motions for a real VIA robot arm

In the following, the approach to experimentally validate the insights obtained from simulations and the developed controller is described. Therefore, we used the VIA robot DLR Hand Arm System which is equipped with seven variable impedance actuators. As the described analysis considers two joints, the robotic arm was configured such that only two joint axes were parallel. Furthermore, the two joint axes pointed in the direction of gravity to remove gravitational effects[4]. Thus, for the experiments the robotic arm structurally corresponded to the system analyzed in the last sections.

[4]This configuration is chosen to be consistent with the simulation analysis.

The bang-bang regulator (9) was used to generate the desired motor position of the first joint, while the measured spring torque of the same joint was the input of the controller. The desired motor position of the second joint (and all other joints not involved in the motions) were constant. Since motor positions are not directly accessible, a motor position PD controller tracked the desired trajectory (desired motor torques were commanded to the current controllers of the motors). Nonzero initial conditions were set manually by pushing the robot by hand.

Phase plots of joint motions are depicted in Fig. 8. Here, approximately four periods in the stationary phase of oscillations are plotted. Furthermore, joint velocities are derived from measured and low-pass filtered joint positions (10 Hz cut-off frequency). The shape of closed paths obtained by experiments is similar to simulations (cf. Fig. 6). The modal properties of the linearized system (in the initial configuration) are about $\omega = (5, 32)\,\mathrm{rad/s}$ for eigenfrequencies and $\xi = (0.05, 0.30)$ for modal damping factors resulting from the natural, low damping in the spring mechanism. As a consequence of eigenfrequency and modal damping distributions also the real robotic system tends to coordinated cyclic motions, while a simple controller is able to stabilize these oscillations. Thus one can observe that a planar, two joint VIA arm with approximately human like dimensions naturally fulfills the conditions for stable cyclic motions.

VI. Conclusion and discussion

In this paper, we investigate main principles and requirements of cyclic motions in strongly nonlinear VIA robotic systems. Starting with simple observations of humans controlling oscillations of serial type passive elastic systems, we analyze human motor control and the elastic system properties to validate that humans are able to control nonlinear, multi degree of freedom oscillations easily. Furthermore we conduct extensive experiments with human in the loop simulations, hardware simulations, and experiments on a real robotic system. Afterward, basic control principles observed in humans are transferred to VIA robotic arms and utilized to identify some basic system requirements for intrinsic cyclic motion tendencies. The most important findings are:

1) A control law to stabilize multi degree of freedom oscillations, which is of simple bang-bang structure.
2) Cyclic motion tendencies can be predicted based on eigenmode analysis of the linearized system.
3) Best preconditions for cyclic motion tendencies are different eigenfrequencies and damping of the modes. For desired motion in a specific mode, the modal damping of that mode has to be under critical and the remaining modes have to be over critically damped.

Furthermore, a simple controller is proposed. The multi-step bang-bang controller can excite and hold cyclic motions for variable stiffness actuated robotic systems in a closed loop manner. This is achieved by using the joint torque—representing the state of the plant's dynamics—to adjust control actions. Due to the controller parameters threshold and step amplitude, the amplitude and frequency of resulting oscillations can be adjusted in a certain range, taking the intrinsic dynamic behavior of the plant into account. Moreover, by adjusting the stiffness preset of the VIA joints the limit cycle can be additionally shaped. This way we make use of the intrinsic oscillation properties of the system by exploiting the resonance property. How the VIA stiffness preset can be changed to fit to a predefined task, will be subject of our future work.

Acknowledgment

This work has been partially funded by the European Commission's Sixth Framework Programme as part of the project SAPHARI (grant number 287513). Additionally, the authors would like to thank Jordi Artigas for providing the force feedback device.

Appendix

The modal decomposition is derived from the linearized system

$$\boldsymbol{M}(\boldsymbol{q}_0)\ddot{\boldsymbol{q}} + \boldsymbol{D}_0\dot{\boldsymbol{q}} + \boldsymbol{K}_0\dot{\boldsymbol{q}} = \boldsymbol{0}\,. \tag{15}$$

Therefore the following lemma (based on [14]) is applied:

Lemma 1: Given a symmetric and positive definite matrix $\boldsymbol{A} \in \mathbb{R}^{n\times n}$ and a symmetric matrix $\boldsymbol{B} \in \mathbb{R}^{n\times n}$. Then there exist a non-singular matrix $\boldsymbol{\Psi} \in \mathbb{R}^{n\times n}$ and a diagonal matrix $\boldsymbol{B}_Q \in \mathbb{R}^{n\times n}$, such that $\boldsymbol{\Psi}^{-T}\boldsymbol{\Psi}^{-1} = \boldsymbol{A}$ and $\boldsymbol{\Psi}^{-T}\boldsymbol{B}_Q\boldsymbol{\Psi}^{-1} = \boldsymbol{B}$.
This leads to the quasi decoupled dynamics in modal coordinates

$$\ddot{\boldsymbol{z}} + \boldsymbol{D}_{mod}(\boldsymbol{q}_0)\dot{\boldsymbol{z}} + \boldsymbol{\Lambda}(\boldsymbol{q}_0)\boldsymbol{z} = \boldsymbol{0}\,, \tag{16}$$

where $\boldsymbol{z} = \boldsymbol{\Psi}(\boldsymbol{q}_0)^{-1}\boldsymbol{q}$ are modal coordinates and $\boldsymbol{\Lambda}(\boldsymbol{q}_0)$ is a diagonal matrix composed of real, positive eigenvalues. The modal damping matrix $\boldsymbol{D}_{mod}(\boldsymbol{q}_0) = \boldsymbol{\Psi}(\boldsymbol{q}_0)^T\boldsymbol{D}_0\boldsymbol{\Psi}(\boldsymbol{q}_0)$ is assumed to be diagonal dominant. Therefore the off diagonal elements are neglected, i.e. $\boldsymbol{d}_{mod}(\boldsymbol{q}_0) = \mathrm{diag}(\boldsymbol{D}_{mod}(\boldsymbol{q}_0))$. Thus, the modal dynamics can be re-written as

$$\ddot{z}_i + 2\xi_i(\boldsymbol{q}_0)\omega_i(\boldsymbol{q}_0)\dot{z}_i + \omega_i(\boldsymbol{q}_0)^2 z_i = 0\,, \tag{17}$$

where

$$\omega_i(\boldsymbol{q}_0) = \sqrt{\mathrm{diag}(\boldsymbol{\Lambda}(\boldsymbol{q}_0))_i}\,, \tag{18}$$

represents the ith eigenfrequency and

$$\xi_i(\boldsymbol{q}_0) = \frac{d_{mod,i}(\boldsymbol{q}_0)}{2\omega_i(\boldsymbol{q}_0)}\,, \tag{19}$$

the normalized damping factor of the ith eigenmode. Conversely, physical damping is assigned by:

$$\boldsymbol{D}_0(\boldsymbol{q}_0) = 2\boldsymbol{\Psi}^{-T}\mathrm{diag}\left(\xi_i(\boldsymbol{q}_0)\omega_i(\boldsymbol{q}_0)\right)\boldsymbol{\Psi}^{-1}\,. \tag{20}$$

The eigenfrequencies of the linearized, conservative system

$$\boldsymbol{M}_0\ddot{\boldsymbol{q}} + \boldsymbol{K}_0\boldsymbol{q} = \boldsymbol{0}\,, \tag{21}$$

are assigned by the solution of the following equality:

$$\det\left(-\lambda\boldsymbol{M} + \boldsymbol{K}_0\right) = \prod_{i=1}^{n}\left(\lambda - \omega_i^2\right) \tag{22}$$

Solving this equation involves dependencies in the choice of ω_i and the structure of $\boldsymbol{K}_0$. Similar eigenfrequencies ω_i require

the stiffness matrix $\boldsymbol{K}_0$ to be fully coupled [17], while the stiffness matrix of most VIA robot arms is diagonal.

In the following, the case $n = 2$ is worked out. Therefore, a nonlinear coupled spring function is derived from the potential function

$$\begin{aligned} U(\theta, \boldsymbol{q}) = &\frac{1}{2}\alpha_1 (q_1 - \theta)^2 + \frac{1}{4}\beta_1 (q_1 - \theta)^4 + \frac{1}{2}\alpha_2 q_2^2 + \frac{1}{4}\beta_2 q_2^4 \\ &+ \frac{1}{2}\alpha_3 (q_2 - (q_1 - \theta))^2 + \frac{1}{4}\beta_3 (q_2 - (q_1 - \theta))^4 \ , \end{aligned} \tag{23}$$

where the negative gradient

$$\begin{aligned} -\left(\frac{\partial U(\theta, \boldsymbol{q})}{\partial \boldsymbol{q}}\right)^T &= \boldsymbol{\psi}(\theta, \boldsymbol{q}) \ , \\ \psi_1(\theta, \boldsymbol{q}) &= -\alpha_1 (q_1 - \theta) - \beta_1 (q_1 - \theta)^3 \\ &\quad + \alpha_3 (q_2 - (q_1 - \theta)) + \beta_3 (q_2 - (q_1 - \theta))^3 \ , \\ \psi_2(\theta, \boldsymbol{q}) &= -\alpha_2 q_2 - \beta_2 q_2^3 \\ &\quad - \alpha_3 (q_2 - (q_1 - \theta)) - \beta_3 (q_2 - (q_1 - \theta))^3 \ , \end{aligned} \tag{24}$$

represents the force field and the negative Jacobian

$$\begin{aligned} -\frac{\partial \boldsymbol{\psi}(\theta, \boldsymbol{q})}{\partial \boldsymbol{q}} &= \boldsymbol{K}(\theta, \boldsymbol{q}) \ , \\ K_{11}(\theta, \boldsymbol{q}) &= \alpha_1 + 3\beta_1 (q_1 - \theta)^2 + \alpha_3 + 3\beta_3 (q_2 - (q_1 - \theta))^2 \ , \\ K_{22}(\theta, \boldsymbol{q}) &= \alpha_2 + 3\beta_2 q_2^2 + \alpha_3 + 3\beta_3 (q_2 - (q_1 - \theta))^2 \ , \\ K_{12}(\theta, \boldsymbol{q}) &= K_{21}(\theta, \boldsymbol{q}) = -\alpha_3 - \beta_3 (q_2 - (q_1 - \theta))^2 \ , \end{aligned} \tag{25}$$

the stiffness matrix.

Equation (22) is solved for α_i by substituting the linearized stiffness matrix

$$\boldsymbol{K}_0 = \begin{bmatrix} \alpha_1 + \alpha_3 & -\alpha_3 \\ -\alpha_3 & \alpha_2 + \alpha_3 \end{bmatrix} , \tag{26}$$

and equating powers of λ:

$$-\frac{\det(-\boldsymbol{M} + \boldsymbol{K}_0) - \det(\boldsymbol{M}) - \det(\boldsymbol{K}_0)}{\det(\boldsymbol{M})} = \omega_1^2 + \omega_2^2 \ , \tag{27}$$

$$\frac{\det(\boldsymbol{K}_0)}{\det(\boldsymbol{M})} = \omega_1 \omega_2 \ . \tag{28}$$

We obtain quadratic equations in powers of α_i, which are solvable for α_1 and α_2, while α_3 is a free parameter:

$$\alpha_1 = \frac{1}{2M_{22}} \left(\left(\omega_1^2 + \omega_2^2\right) \det(\boldsymbol{M}) - 2 (M_{22} + M_{12}) \alpha_3 \pm \sqrt{\mu} \right) \ , \tag{29}$$

$$\alpha_2 = \frac{1}{2M_{11}} \left(\left(\omega_1^2 + \omega_2^2\right) \det(\boldsymbol{M}) - 2 (M_{11} + M_{12}) \alpha_3 \pm \sqrt{\mu} \right) \ , \tag{30}$$

$$\begin{aligned} \mu = &\left(\omega_1^2 - \omega_2^2\right)^2 \det(\boldsymbol{M})^2 - 4\omega_1^2 \omega_2^2 M_{12}^2 \det(\boldsymbol{M}) \\ &- 4 \det(\boldsymbol{M}) \left(M_{12} \left(\omega_1^2 + \omega_2^2\right) + \alpha_3 \right) \alpha_3 \ . \end{aligned} \tag{31}$$

The spring constants α_1 and α_2 have to be real. Additionally, the stiffness matrix $\boldsymbol{K}_0$ has to be positive definite; consequently α_3 has to be chosen such that the discriminant $\mu \geq 0$ and the minor eigenvalue of the stiffness matrix $\min(\mathrm{eig}(\boldsymbol{K}_0)) > 0$.

As a consequence of the coupled mass matrix, the stiffness matrix has to be non-diagonal (i.e., $\alpha_3 \neq 0$) if the ratio of the assigned eigenfrequencies $\nu = \omega_2/\omega_1$ undercuts the greatest lower bound $\nu_{\min}(\boldsymbol{M})$. This property can be proven by substituting $\alpha_3 = 0$ in (31) and solving for the ratio ω_2/ω_1:

$$\nu_{\min}(\boldsymbol{M}) = \frac{\sqrt{\det(\boldsymbol{M}) + 2M_{12}^2 + 2M_{12}\sqrt{M_{12}^2 + \det(\boldsymbol{M})}}}{\sqrt{\det(\boldsymbol{M})}} \ . \tag{32}$$

References

[1] Grebenstein and Smagt, "Antagonism for a highly anthropomorphic hand-arm system," *Advanced Robotics*, vol. 22, no. 1, pp. 39–55, 2008.

[2] Albu-Schäffer *et al.*, "Anthropomorphic soft robotics from torque control to variable intrinsic compliance," in *Robotics Research*, ser. Springer Tracts in Advanced Robotics, Pradalier, Siegwart, and Hirzinger, Eds. Springer Berlin / Heidelberg, 2011, vol. 70, pp. 185–207.

[3] Visser, Stramigioli, and Bicchi, "Embodying desired behavior in variable stiffness actuators," in *2011 Congress of the International Federation of Automatic Control - IFAC 2011*, 2011.

[4] Garabini, Passaglia, Belo, Salaris, and Bicchi, "Optimality principles in variable stiffness control: The vsa hammer." in *IEEE/RSJ Int. Conf. on Intelligent Robots and Systems*, 2011, pp. 3770–3775.

[5] Braun, Howard, and Vijayakumar, "Exploiting variable stiffness in explosive movement tasks," in *Robotics: Science and Systems*, 2011.

[6] Haddadin, Huber, and Albu-Schäffer, "Optimal control for exploiting the natural dynamics of variable stiffness robots," in *IEEE Int. Conf. on Robotics and Automation*, 2012.

[7] Nayfeh and Mook, *Nonlinear Oscillations*. John Wiley & Sons, 1979.

[8] Guckenheimer and Holmes, *Nonlinear Oscillations, Dynamical Systems, and Bifurcations of Vector Fields*. Springer–Verlag, 1983.

[9] Albu-Schäffer, Wolf, Eiberger, Haddadin, Petit, and Chalon, "Dynamic modelling and control of variable stiffness actuators," in *IEEE Int. Conf. on Robotics and Automation*, 2010.

[10] Albu-Schäffer, Ott, and Petit, "Constructive energie shaping control for a class of euler-lagrange systems," in *10th Int. IFAC Symposium on Robot Control*, 2012.

[11] Grebenstein *et al.*, "The DLR Hand Arm System," in *Proc. IEEE Int. Conf. on Robotics and Automation*, 2011.

[12] Wolf and Hirzinger, "A new variable stiffness design: Matching requirements of the next robot generation," in *Proc. IEEE Int. Conf. on Robotics and Automation*, 2008.

[13] Hoffer, Stein, Haugland, Sinkjaer, Durfee, Schwartz, Loeb, and Kantor, "Neural signals for command control and feedback in functional neuromuscular stimulation: a review." *Journal of Rehabilitation Research and Development*, vol. 33, no. 2, pp. 145–157, Apr. 1996.

[14] Ott, *Cartesian Impedance Control of Redundant and Flexible-Joint Robots*, Siciliano and Khatib, Eds. Springer, 2008.

[15] Kokotovic, Khalil, and O'Reilly, *Singular Perturbation Methods in Control: Analysis and Design*. Academic Press, London, 1986.

[16] Khalil, *Nonlinear Systems, 3rd edn.* Prentice Hall, Englewood Cliffs, 2002.

[17] Petit, Lakatos, Friedl, and Albu-Schäffer, "Dynamic trajectory generation for serial elastic actuated robots," in *10th Int. IFAC Symposium on Robot Control*, 2012.